isvr Institute of Sound and Vibration Research

# Plane Wave Decomposition of the Sound Field on a Sphere by Spherical Convolution

**B. Rafaely**

ISVR Technical Memorandum 910

May 2003

University of Southampton

# SCIENTIFIC PUBLICATIONS BY THE ISVR

***Technical Reports*** are published to promote timely dissemination of research results by ISVR personnel. This medium permits more detailed presentation than is usually acceptable for scientific journals. Responsibility for both the content and any opinions expressed rests entirely with the author(s).

***Technical Memoranda*** are produced to enable the early or preliminary release of information by ISVR personnel where such release is deemed to the appropriate. Information contained in these memoranda may be incomplete, or form part of a continuing programme; this should be borne in mind when using or quoting from these documents.

***Contract Reports*** are produced to record the results of scientific work carried out for sponsors, under contract. The ISVR treats these reports as confidential to sponsors and does not make them available for general circulation. Individual sponsors may, however, authorize subsequent release of the material.

UNIVERSITY OF SOUTHAMPTON

INSTITUTE OF SOUND AND VIBRATION RESEARCH

SIGNAL PROCESSING & CONTROL GROUP

# Plane Wave Decomposition of the Sound Field on a Sphere by Spherical Convolution

by

**Boaz Rafaely**

ISVR Technical Memorandum N° 910

May 2003

Authorised for issue by
Prof S J Elliott
Group Chairman

# Plane wave decomposition of the sound field on a sphere by spherical convolution

Boaz Rafaely*

*Institute of Sound and Vibration Research,*

*University of Southampton, Southampton SO17 1BJ, UK*

(Dated: 2 May, 2003)

Abbreviated title: Wave decomposition by spherical convolution.

*Email: br@isvr.soton.ac.uk

Abstract

Spherical microphone arrays have been recently studied for sound analysis and sound recordings, which have the advantage of spherical symmetry facilitating three-dimensional analysis. This paper complements the recent microphone array design studies by presenting a theoretical analysis of plane wave decomposition given the sound pressure on a sphere. The analysis uses the spherical Fourier transform and the spherical convolution, where it is shown that the amplitudes of the incident plane waves can be calculated as a spherical convolution between the pressure on the sphere and another function which depends on frequency and the sphere radius. This is in contrast to planar configuration, where the waves amplitudes and the pressure on a plane form a Fourier transform pair. The spatial resolution of plane wave decomposition given limited bandwidth in the spherical Fourier domain is analyzed, and shown to be similar to the spatial resolution for planar configuration with finite aperture. The paper concludes with a simulation example of plane wave decomposition.

PACS numbers: 43.60.Ac, 43.60.Fy, 43.55.Br, 43.55.Mc

## I. INTRODUCTION

Reverberant sound fields have been widely studied, as they have a significant influence on the acoustic performance of enclosures in a variety of applications. For example, the intelligibility of speech in lecture rooms; the quality of music in auditoria; and the noise level in offices, are all affected by the enclosed sound field. Systems that measure reverberant sound fields or operate in such fields often require microphone arrays to achieve the high spatial detail imposed by the complexity of the sound field. Linear and planar microphone arrays are commonly used, and have have a well developed theoretical analysis. For example, decomposition into plane waves can be achieved with infinitely large linear or planar arrays by the spatial Fourier transform. Furthermore, directivity due to a single wave "spreads" from a delta function to a sinc function when the array aperture is made finite[1]. Some example applications involving linear and planar microphone arrays include speech enhancement and speaker tracking in conference rooms[2,3]; auralization of sound fields measured in concert halls[4]; and the study and modifications of sound fields in auditoria[5,6].

Recently, spherical microphone arrays have been suggested for spatial beamforming[7–9] and for sound recordings with high spatial detail[10,11]. The advantage of the spherical microphone array configuration is the spherical symmetry which facilitates three dimensional sound field analysis. Gover et al[12] recently presented a measurement system based on spherical microphone arrays for the analysis of reverberant sound fields using various spatial measures. Beamforming is employed with the beam steered electronically to cover all directions therefore providing complete three-dimensional sound field analysis.

The recent developments in spherical microphone arrays motivated the work presented in this paper. Although useful microphone array designs and applications have been presented in previous papers, they do not provide a theoretical analysis similar to that available for linear and planar arrays. The aim of this work is therefore the theoretical analysis of spherical microphone arrays, with a focus on plane wave decomposition and fundamental limits of performance. Two simplifying assumptions are made:

(i) The sound pressure on the entire sphere is known. Although this is usually not true in practice, this assumption simplifies the development of the theoretical results. The discussion of spatial sampling by microphones is beyond the scope of this paper, although the reader is referred to Driscoll and Healy[13] for a discussion and a sampling

theorem.

(ii) The sound field is composed of plane waves. This will be approximately true in reverberant sound fields for waves which have traveled sufficient distance from their source.

Given these assumptions, we show that the relation between the pressure on a sphere and the complex amplitude of the plane waves composing the sound field around the sphere is that of spherical convolution. In other words, plane wave decomposition is achieved by convolving the pressure on a sphere with another function which depends only on frequency and the sphere radius. This is in contrast to linear and planar array configurations, where the directivity of the sound field is given by the Fourier transform of the pressure on the line or plane[1]. We also show that perfect pane wave decomposition requires infinite number of spherical Fourier coefficients, or an infinite spherical harmonic order. We then derive an expression for the spatial resolution in the more practical case where the harmonic order is finite, and compare the results to the spatial resolution of a finite aperture planar array.

The paper is presented as follows. Section II presents the spherical Fourier transform and the spherical convolution, and develops important relations that will be used later in the paper. The sound pressure on the sphere is then analyzed in section III, and represented as a spherical convolution between the plane waves amplitude and another function. Plane wave decomposition is then developed in section IV by de-convolution of the pressure, or convolution with the inverse function. The effect of finite order or bandwidth in the spherical Fourier domain on the resolution of plane wave decomposition is presented in section V, and a comparison between spherical and planar configurations is presented in section VI. The paper then concludes with a simulation example of plane wave decomposition in section VII.

## II. SPHERICAL FOURIER TRANSFORM

The spherical Fourier transform[13], or spherical harmonics decomposition[1] is reviewed in this section. In particular, the Fourier transform and convolution on the sphere, and some properties of spherical harmonics are presented which are then used in the derivations that follow.

The standard cartezian $(x, y, z)$ and spherical $(r, \theta, \phi)$ coordinate systems as used through-

out this paper are illustrated in Fig. 1. Consider a function $f(\theta,\phi)$ which is square integrable on the unit sphere, then the spherical Fourier transform of $f$, denoted by $\tilde{f}_{nm}$ is given by[13]:

$$\tilde{f}_{nm} = \int_{\Omega\in S^2} f(\theta,\phi)Y_n^{m^*}(\theta,\phi)d\Omega = \mathcal{S}\left\{f(\theta,\phi)\right\} \tag{1}$$

$$f(\theta,\phi) = \sum_{n=0}^{\infty}\sum_{m=-n}^{n} \tilde{f}_{nm}Y_n^m(\theta,\phi) = \mathcal{S}^{-1}\left\{\tilde{f}_{nm}\right\} \tag{2}$$

where $\mathcal{S}$ and $\mathcal{S}^{-1}$ represent the forward and inverse spherical Fourier transforms respectively, and "*" represents complex conjugate. The spherical harmonics $Y_n^m$ are defined by:

$$Y_n^m(\theta,\varphi) \equiv \sqrt{\frac{(2n+1)}{4\pi}\frac{(n-m)!}{(n+m)!}}P_n^m(\cos\theta)e^{im\phi} \tag{3}$$

where $n$ is the order of the spherical harmonics and $i=\sqrt{-1}$. The spherical harmonics are the solution to the wave equation, or the Helmholtz equation in spherical co-ordinates[1,14]. The associated Legendre function $P_n^m$ represents standing spherical waves in $\theta$ while the term $e^{im\phi}$ represents traveling spherical waves in $\phi$. The integral $\int_{\Omega\in S^2} d\Omega$ covers the entire surface area of the unit sphere, denoted by $S^2$, and is expressed as[1]:

$$\int_{\Omega\in S^2} d\Omega = \int_0^{2\pi}\int_0^{\pi} \sin\theta d\theta\, d\phi \tag{4}$$

Some properties of spherical harmonics and the spherical Fourier transform which are used in the derivations that follow are presented below.

### A. Orthogonality

The spherical harmonics are orthonormal, and so the following relations hold[14]:

$$\mathcal{S}\left\{Y_{n'}^{m'}(\theta,\phi)\right\} = \int_{\Omega\in S^2} Y_{n'}^{m'}(\theta,\phi)Y_n^{m^*}(\theta,\phi)d\Omega = \delta_{n-n'}\delta_{m-m'} \tag{5}$$

$$\begin{aligned}\mathcal{S}^{-1}\left\{Y_n^{m^*}(\theta',\phi')\right\} &= \sum_{n=0}^{\infty}\sum_{m=-n}^{n} Y_n^{m^*}(\theta',\phi')Y_n^m(\theta,\phi) \\ &= \delta(\phi-\phi')\delta(\cos\theta-\cos\theta') = \frac{1}{\sin\theta}\delta(\phi-\phi')\delta(\theta-\theta')\end{aligned} \tag{6}$$

where $\delta_{n-n'}$ and $\delta_{m-m'}$ are unity at $n = n'$ and $m = m'$ respectively, and zero elsewhere, and similarly, $\delta(\phi - \phi')$ and $\delta(\theta - \theta')$ are infinite at $\phi = \phi'$ and $\theta = \theta'$ and zero elsewhere.

### B. Complex conjugation

The following relation between a spherical harmonic and its complex conjugate holds[13]:

$$Y_n^{m^*} = (-1)^m Y_n^{-m} \tag{7}$$

### C. Phase shift

Given a direction denoted by $(\theta, \phi)$, then the opposite direction is given by $(\pi - \theta, \phi + \pi)$. The relation between the spherical harmonics at point of opposite directions is given by[15]:

$$Y_n^m(\pi - \theta, \phi + \pi) = (-1)^n Y_n^m(\theta, \phi) \tag{8}$$

Also, from the two relations[15] $Y_n^m(\theta, -\phi) = (-1)^m Y_n^{-m}(\theta, \phi)$ and $Y_n^m(\theta, \pi + \phi) = (-1)^m Y_n^m(\theta, \phi)$, the following relation for a phase inversion and shift in $\phi$ can be derived:

$$Y_n^m(\theta, \pi - \phi) = Y_n^{-m}(\theta, \phi) \tag{9}$$

### D. Azimuthal symmetry

In this section the relations between the Fourier coefficients of a function and its symmetry on the sphere with respect to the azimuth $\phi$ are established. First, consider a function $h$ on the sphere with coefficients which are zero for all $m \neq 0$, i.e. $\tilde{h}_{nm} = \tilde{h}_n \delta_m$. In this case we can show that the function is constant along $\phi$, i.e.

$$\tilde{h}_{nm} = \tilde{h}_n \delta_m \quad \Leftrightarrow \quad h(\theta, \phi) = h(\theta) \tag{10}$$

This is since the integral over $\phi$ in Eq. (1) reduces in this case to $\int_0^{2\pi} e^{im\phi} d\phi = \delta_m$. while the summation in Eq. (2) reduces to a single summation over $n$ which is not a function of $\phi$.

Another type of symmetry is considered when $\tilde{h}_{nm} = \tilde{h}_{n(-m)}$. Evaluating $h(\theta, \pi - \phi)$ in Eq. (2), and substituting Eq. (9) and $\tilde{h}_{nm} = \tilde{h}_{n(-m)}$, it can be shown that:

$$\tilde{h}_{nm} = \tilde{h}_{n(-m)} \quad \Leftrightarrow \quad h(\theta, \phi) = h(\theta, \pi - \phi) \tag{11}$$

This means that symmetry over $m = 0$ results in symmetry over $\phi$ with the symmetry points $\phi = 90°$ and $\phi = 270°$.

When the Fourier coefficients are equal for all $m$, i.e. $\tilde{h}_{nm} = \tilde{h}_{n0} = \tilde{h}_n$, then $h$ can be evaluated in terms of the two symmetry properties discussed above. First, the values of $\tilde{h}_{nm}$ for $m = 0$ correspond to the part in $h$ which is constant with $\phi$. Then, as the coefficients are all constant with respect to $m$. $\tilde{h}_{nm} = \tilde{h}_{n(-m)}$ is satisfied and so the function is symmetric along $\phi$ around the symmetry points $\phi = 90°, 270°$. This result will be used later in this paper.

### E. Convolution

Driscoll and Healy[13] show that the spherical Fourier transform converts convolution into multiplication. As this is a result which is key to this paper, the spherical convolution is described in an appropriate detail. Consider two functions $f(\gamma)$ and $h(\gamma)$ square integrable on the unit sphere, with the vector of cartezian coordinates $\gamma(\theta, \phi) = (\sin\theta\cos\phi, \sin\theta\sin\phi, \cos\theta)^T$ representing a point on the unit sphere. The convolution of $f$ with $h$ denoted by $e = f * h$ is defined[13] in a similar way to the convlution over a line or a plane, as the integral of the product of $f$ and a rotated $h$, for all possible rotations,

$$e(\gamma) = (f * h)(\gamma) = \int_{g \in SO(3)} f(g\eta) h(g^{-1}\gamma) dg \tag{12}$$

where the special orthogonal group of $3 \times 3$ matrices, $SO(3)$, represents the three dimensional rotation group, with $g \in SO(3)$ spanning all rotations, and $\eta = (0, 0, 1)^T$ is the north pole. Euler matrix representation of rotation can be used[13], where

$$g = R_z(\phi) R_y(\theta) R_z(\psi) \tag{13}$$

The $3 \times 3$ matrix $R_z(\phi)$ represents a counterclockwise rotation by an angle $\phi$ about the

$z$ axis, while the matrix $R_y(\theta)$ represents a counterclockwise rotation by an angle $\theta$ about the $y$ axis, and are given by[13]

$$R_z(\phi) = \begin{pmatrix} \cos\phi & -\sin\phi & 0 \\ \sin\phi & \cos\phi & 0 \\ 0 & 0 & 1 \end{pmatrix}, \; R_y(\theta) = \begin{pmatrix} \cos\theta & 0 & \sin\theta \\ 0 & 1 & 0 \\ -\sin\theta & 0 & \cos\theta \end{pmatrix} \tag{14}$$

Note that the rotation matrices are defined in cartezian coordinates, e.g. $R_z$ rotates a point $(x, y, z)$ to the point $(x', y', z')^T = R_z(\phi)(x, y, z)^T$. $R_z(\psi)$ is defined similarly to $R_z(\phi)$. The inverse of $g$ in Eq. (12) can be written as[14]:

$$g^{-1} = g^T = R_z(-\psi)R_y(-\theta)R_z(-\phi) \tag{15}$$

The position defined by $g\eta$ in Eq. (12) simplifies to $(\theta, \phi)$ in spherical coordinates[13], i.e.

$$g\eta = (\sin\theta\cos\phi, \sin\theta\sin\phi, \cos\theta)^T \tag{16}$$

Representing rotations by the Euler angles, the rotation integral can be written as[13]:

$$\int_{g\in SO(3)} dg = \int_0^{2\pi}\int_0^{2\pi}\int_0^{\pi} \sin\theta \, d\theta \, d\phi \, d\psi \tag{17}$$

Driscoll and Healy[13] show that spherical convolution converts to multiplication through the spherical Fourier transform, i.e.

$$\begin{aligned} \tilde{e}_{nm} &= \mathcal{S}\{e(\gamma)\} = \mathcal{S}\{f(\gamma) * h(\gamma)\} = \int_{\gamma\in S^2}\int_{g\in SO(3)} f(g\eta)h(g^{-1}\gamma)Y_n^{m^*}(\gamma)\, dg\, d\gamma \\ &= \tilde{f}_{nm} \cdot \tilde{h}_{n0} \end{aligned} \tag{18}$$

where $\tilde{f}_{nm} = \mathcal{S}\{f\}$ and $\tilde{h}_{nm} = \mathcal{S}\{h\}$. Note that $\tilde{h}_{nm}$ is evaluated only at $m = 0$. This means that $f * g \neq g * h$ and so the spherical convolution is non-commutative, or non-abelian. The convolution $f * h$ is denoted the left convolution[13] of $h$ by $f$. Also note that an alternative definition of spherical convolution exists[16], although the one presented here was found to be more useful in this paper.

Eqaution (18) suggests that only the coefficients $\tilde{h}_{n0}$ which correspond to the azimuthally symmetric part of $h$ participate in the convolution. The function with Fourier coefficients $\tilde{h}_{n0}$ is symmetric along $\phi$ in a manner described in section II D.

## III. THE SOUND PRESSURE ON A SPHERE

In this section the sound pressure measured on a sphere is derived given the sound field around the sphere. The results are then combined in the next section with the results on spherical convolution in the formulation of plane wave decomposition. As the sound field is assumed to be composed of plane waves, the pressure on a sphere for such sound field is derived .

Consider an incident plane wave arriving from a direction denoted by $(\theta_l, \phi_l)$, with amplitude $w(\theta_l, \phi_l)$. The wave therefore propagates in the direction given by $(\pi - \theta_l, \phi_l + \pi)$. The pressure on an open sphere (virtual sphere) due to the incident plane wave at the position $\mathbf{r} = (r, \theta, \phi)$ and wave-number $k$, denoted by $p_l(kr, \theta, \phi)$, can be written using spherical harmonics as[1]:

$$p_l(kr, \theta, \phi) \;=\; w(\theta_l, \phi_l) e^{j\mathbf{k}_l \cdot \mathbf{r}} = w(\theta_l, \phi_l) \sum_{n=0}^{\infty} \sum_{m=-n}^{n} 4\pi (-i)^n j_n(kr) Y_n^{m^*}(\theta_l, \phi_l) Y_n^m(\theta, \phi) \quad (19)$$

where $\mathbf{k}_l$ is the wave number vector representing the direction of propagation of the wave, with $k = |\mathbf{k}_l|$. Note that Williams[1] (page 227) represents a similar equation in terms of the direction of propagation of the plane wave. Equation (19) was derived from the one given by Williams by using the relation in Eq. (8), and so $(\theta_l, \phi_l)$ represents the direction of arrival. If the sphere is rigid, then a scattered pressure from the sphere will be added to the incident pressure (which is equal to the open sphere case, Eq. (19)). The boundary condition on the rigid sphere (normal velocity equal zero) is substituted into Euler's equation (expressing velocity as the gradient of pressure), to calculate the coefficients of the scattered field and therefore the total field. A derivation can be found in Williams[1] (page 226), and the pressure in this case is given by:

$$p_l(kr, \theta, \phi) = \sum_{n=0}^{\infty} \sum_{m=-n}^{n} w(\theta_l, \phi_l) \tilde{b}_n(kr, ka) Y_n^{m^*}(\theta_l, \phi_l) Y_n^m(\theta, \phi) \quad (20)$$

where $\tilde{b}_n$ is generalized for both the open and rigid sphere cases:

$$\tilde{b}_n(kr, ka) = \begin{cases} 4\pi(-i)^n \left( j_n(kr) - \frac{j_n'(ka)}{h_n'(ka)} h_n(kr) \right) & \textit{rigid sphere} \\ 4\pi(-i)^n j_n(kr) & \textit{open sphere} \end{cases} \quad (21)$$

where $h_n(kr)$ is a spherical Bessel function (also denoted by $h_n^{(1)}$), and $a \leq r$ is the radius of the rigid sphere.

Tasking the spherical Fourier transform (as in Eq. (1)) of Eq. (20), the coefficients $\tilde{p}_{l_{nm}}$ are given by:

$$\tilde{p}_{l_{nm}}(kr) = w(\theta_l, \phi_l)\tilde{b}_n(kr, ka)Y_n^{m^*}(\theta_l, \phi_l) \tag{22}$$

We now assume that an infinite number of plane waves arrive at the sphere from all directions $\Omega_l = (\theta_l, \phi_l)$. The total pressure on a sphere of radius $r$ due to all waves can be calculated by integrating Eq. (20) over these directions:

$$\begin{aligned} p(\theta, \phi) &= \int_{\Omega_l \in S^2} p_l(\theta_l, \phi_l) d\Omega_l = \sum_{n=0}^{\infty} \sum_{m=-n}^{n} \tilde{b}_n \left[ \int_{\Omega_l} w(\theta_l, \phi_l) Y_n^{m^*}(\theta_l, \phi_l) d\Omega_l \right] Y_n^m(\theta, \varphi) \\ &= \sum_{n=0}^{\infty} \sum_{m=-n}^{n} \left\{ \tilde{b}_n \widetilde{w}_{nm} \right\} Y_n^m(\theta, \phi) \end{aligned} \tag{23}$$

where the dependence on $k$ has been dropped to simplify notation. From the definitions of the spherical Fourier transform, Eqs. (1) and (2), it is clear that the curly brackets in Eq. (23) represent the Fourier coefficients $\tilde{p}_{nm}$ of the pressure $p$, while the term in the square brackets represent the Fourier coefficients $\widetilde{w}_{nm}$ of the sound field directivity function $w$. They are therefore related by the term $\tilde{b}_n$, i.e.

$$\tilde{p}_{nm} = \widetilde{w}_{nm}\tilde{b}_n \tag{24}$$

Equation (24) has the same form as Eq. (18), where we set $\tilde{b}_{n0} = \tilde{b}_n$. Because in this case the coefficients $\tilde{b}_{nm}$ are equal for all $m$, and are therefore simply denoted by $\tilde{b}_n$, the multiplication in Eq. (24) transform into convolution as in Eq. (12). Therefore, the pressure on the sphere can be written as a spherical convolution between the directivity function $w$ and the inverse spherical Fourier transform of $\tilde{b}_n$:

$$p = w * b \tag{25}$$

where

$$b = \mathcal{S}^{-1}\left\{ \tilde{b}_n \right\} \tag{26}$$

Note that $w$ for the case of a single plane wave as used in Eq. (19) represents sound pressure amplitude, while $w$ for the case of an infinite number of plane waves, as used in Eq. (20) represents sound pressure amplitude density (spatial density with respect to the solid angle). For notation simplicity, they are both denoted $w$.

## IV. PLANE WAVE DECOMPOSITION

Equation (24) can be rewritten as:

$$\widetilde{w}_{nm} = \tilde{p}_{nm} \cdot \frac{1}{\tilde{b}_n} \tag{27}$$

By taking the inverse spherical Fourier transform of both sides and using the result in Eq. (18), we can write the relation between the the amplitude of the incoming plane waves and the pressure measured on the sphere, i.e. the plane wave decomposition, as spherical convolution:

$$w = p * \beta \tag{28}$$

where

$$\beta = \mathcal{S}^{-1}\left\{\frac{1}{\tilde{b}_n}\right\} \tag{29}$$

Plane wave decomposition, or $w$ can therefore be found by de-convolution of $p$ with $b$, or by convolution of $p$ with $\beta$.

Taking the simple case of a single plane wave with a unit amplitude arriving from direction $(\theta_l, \phi_l)$, we can substitute Eq. (22) in Eq. (28), and use the orthogonality property of the spherical harmonics (Eq. 6) to get:

$$\begin{aligned} w(\theta,\phi) &= \sum_{n=0}^{\infty}\sum_{m=-n}^{n}\left\{\tilde{p}_{nm}\frac{1}{\tilde{b}_n}\right\}Y_n^m(\theta,\phi) \\ &= \sum_{n=0}^{\infty}\sum_{m=-n}^{n} Y_n^{m*}(\theta_l,\phi_l)Y_n^m(\theta,\phi) = \delta(\phi-\phi_l)\delta(\cos\theta-\cos\theta_l) \end{aligned} \tag{30}$$

This confirms that the directivity of a single plane wave is a delta function pointing to the arrival direction of the plane wave.

Figures 2a and 2b show $\tilde{b}_n(kr, kr)$ for a rigid and an open sphere, respectively, as a function of $kr$ and the order $n$. It is clear that terms with higher order have smaller magnitude, while for the rigid sphere, terms with order higher then about $kr$ contribute significantly less than the lower order terms. Figure 2b shows that for an open sphere, some coefficients $\tilde{b}_n$ will be zero for some values of $kr$, and so Eq. (28), which uses Eq. (29) and $1/\tilde{b}_n$ cannot be used. This is not the case for a rigid sphere, and so the advantage of the rigid sphere in providing a better conditioned problem is clear. Figure 3 further illustrates $\tilde{b}_n$ for a rigid sphere and several values of $ka$, showing clearly how $\tilde{b}_n$ starts to decay in magnitude beyond about $n = ka$.

As an example and to illustrate functions $b$ and $\beta$ for a rigid sphere, they are calculated for $kr = ka = 5$ and $n \leq 10$ using Eq. (2), and evaluated over a finite grid on the unit sphere. Figures 4a and 4b show $b(\theta, \phi)$ using a 3D plot on a unit sphere, and on a 2D plot as a function of $\theta$ and $\phi$. Note the symmetry around $\phi = 90°$ and $\phi = 270°$, as expected from the symmetry property presented in Eq. (11) satisfied by $\tilde{b}_n$.

For band-limited $p$, i.e. $\tilde{p}_{nm} = 0$ for $n > N$, the corresponding $w$ is also band-limited as evident from Eq. (27). This means that to find $w$, a band-limited version of $\beta$ is required, i.e. only $1/\tilde{b}_n$ for $n \leq N$ are required. A band-limited version of Eq. (28) can therefore be written as:

$$w_N = p_N * \beta_N \tag{31}$$

where the functions $w_N$, $p_N$ and $\beta_N$ are calculated using the inverse spherical Fourier transform as in Eq. (2) only with the summation over $n$ taken from 0 to $N$ and not infinity. This is a useful result since the calculation of $\beta$ using Eq. (29) involves an inverse of $\tilde{b}_n$, and as illustrated in Fig. 3, $\tilde{b}_n \to 0$ as $n \to \infty$. To ensure stability of $\beta$, $\tilde{b}_n$ must be truncated, and so if $p$ is originally measured over a finite band, $\tilde{b}_n$ is truncated to the same order with no further loss of accuracy in plane wave decomposition. Note from Eq. (22) that $\tilde{b}_n$ also appears in the magnitude of the pressure on the sphere due to a plane wave, and so given the frequency and the sphere dimensions, $kr$, the magnitude of the Fourier coefficients of order larger then $kr$ is expected to diminish, and so the assumption that $p$ is band-limited will be

approximately correct. Nevertheless, as shown in the next section, the spatial resolution of plane wave decomposition depends on the order $N$, and so truncating the bandwidth of $p$ could limit plane wave decomposition.

Figures 5a and 5b presents the corresponding plots for $\beta$, for $n \leq 10$, showing similar symmetry properties over $\phi$

## V. FINITE HARMONIC ORDER AND SPATIAL RESOLUTION

In practice it might not be possible to measure all spherical Fourier coefficients of the pressure, since coefficients which are of order higher then about $kr$ might be too small in magnitude to be computed accurately. Therefore, a finite harmonic order, or finite bandwidth, is considered in this section, and the effect on plane wave decomposition is studied.

The directivity of the sound field can be calculated by taking the inverse spherical Fourier transform of Eq. (27), only with a finite order $N$:

$$w_N(\theta,\phi) = \sum_{n=0}^{N}\sum_{m=-n}^{n} \tilde{p}_{nm}\frac{1}{\tilde{b}_n}Y_n^m(\theta,\phi) \tag{32}$$

We now study the effect of finite order on the estimation of the directivity of a single plane wave with a unit amplitude arriving from $(\theta_l,\phi_l)$, by substituting Eq. (22) in Eq. (32):

$$\begin{aligned} w_N(\theta,\phi) &= \sum_{n=0}^{N}\sum_{m=-n}^{n} \tilde{p}_{nm}\frac{1}{\tilde{b}_n}Y_n^m(\theta,\phi) = \sum_{n=0}^{N}\sum_{m=-n}^{n} Y_n^m(\theta_l,\phi_l)^* Y_n^m(\theta,\phi) = \sum_{n=0}^{N}\frac{2n+1}{4\pi}P_n(\cos\Theta) \\ &= \frac{N+1}{4\pi(\cos\Theta-1)}(P_{N+1}(\cos\Theta)-P_N(\cos\Theta)) = w_N(\Theta) \end{aligned} \tag{33}$$

where $\Theta$ is the angle between the vectors with directions $(\theta,\phi)$ and $(\theta_l,\phi_l)$, which can be written as[14]:

$$\cos\Theta = \cos\theta\cos\theta_l + \cos(\phi-\phi_l)\sin\theta\sin\theta_l \tag{34}$$

The Spherical harmonic addition theorem (Arfken and Weber[14], page 796 and onwards) was used in the first line of Eq. (33), while the second line used a result from Gradshteyn and Ryzhik[17] (page 1026, section 8.915 (1)).

A finite order will result in directivity for a plane wave which is not a delta function, and will compromise plane wave decomposition. Figure 6 shows the directivity $w_N(\Theta)$ for various values of $N$, normalized to have a unit gain at $\Theta = 0$ . It is clear that with higher orders the directivity approaches that of a delta function. Notice that $w_N$ is now only a function of a single angle $\Theta$ around an axis given by the vector $(\theta_l, \phi_l)$.

We now formulate a relation between $N$ and the resolution in the plane wave decomposition, by considering the first zero $\Theta_0$ of $w_N(\Theta)$, and taking twice that value, or the width of the main lobe, as the resolution. This implies that plane waves separated by $2\Theta_0$ should be decomposed reasonably well, where $\Theta_0$ is the smallest value that satisfies $w_N(\Theta_0) = 0$. Equation (33) shows that $w_N$ is a sum of two Legendre polynomials in $\cos\Theta$. We can therefore compute the coefficients of these polynomials for every $N$, find their zeros, and locate the smallest zero $\Theta_0$. As Legendre polynomials $P_n(z)$ are defined over $z \in [-1, 1]$, we find the zero which is nearest to 1 (such that $\cos\Theta$ is nearest zero). It turns out that the polynomial defined by $P_{N+1}(z) - P_N(z)$ has the first zero at $z = 1$, which is cancelled by a pole at $z = 1$, i.e. the term $\cos\Theta - 1$. Therefore the next zero nearest 1 is chosen. Table I shows $w_N$ expressed as a polynomial for $N \leq 5$. This provides an explicit form for the directivity function, although the result in Eq. (33) can be used more generally.

Figure 7 shows $\Theta_0$ as a function of $N$, and as approximated by:

$$\Theta_0 \approx \frac{\pi}{N} \tag{35}$$

The error of this approximation was found to be less then 2° for $N \in [4, 40]$. Assuming that for a given frequency we choose $N = kr$, i.e. neglecting the higher order harmonics which are less significant and more difficult to compute accurately, as discussed above, then a new relation for the width or resolution $2\Theta_0$ can be written using Eq. (35), in term of the sphere radius $r = a$ and the wave number $k$, as:

$$2\Theta_0 \approx \frac{2\pi}{ka} \tag{36}$$

## VI. COMPARING PLANAR AND SPHERICAL CONFIGURATIONS

This section compares the results for plane wave decomposition given the pressure on a sphere, to the already established results of plane wave decomposition given the pressure

on a plane. In particular, it is shown that while the pressure and the directivity functions are related through convolution in the spherical case, they form a Fourier pair in the planar case. Also it is shown that both configurations provide comparable spatial resolution under practical constraints of finite harmonic order for the spherical case and finite aperture for the planar case.

Consider a plane wave of angular frequency $\omega$ propagating in a three dimensional space denoted by the cartezian coordinate system $(x, y, z)$, as in Fig. 1. The wave number scalar $k = \omega/c = 2\pi/\lambda$, with $c$ the speed of sound and $\lambda$ the wavelength, describes the wavelength along the direction of propagation. The wave number vector $\mathbf{k}$ has a magnitude of $k$ and a direction equal the direction of propagation of the plane wave, such that

$$\mathbf{k} = (k_x, k_y, k_z), \qquad |\mathbf{k}| = k = \sqrt{k_x^2 + k_y^2 + k_z^2} \tag{37}$$

The pressure on the plane $z = 0$ at the position vector $\mathbf{x} = (x, y, 0)$ due to a plane wave with a complex amplitude $w(\mathbf{k})$ is given by[1]:

$$p(x, y) = w(k_x, k_y)e^{j\mathbf{k}\cdot\mathbf{x}} = w(k_x, k_y)e^{j(k_x x + k_y y)} \tag{38}$$

where $\{\cdot\}$ is the dot or scalar product. The dependence of $w$ on $k_z$ has been dropped because from Eq. (37) we can write $k_z = \pm\sqrt{k^2 - k_x^2 - k_y^2}$. To eliminate the ambiguity in the direction of arrival (due to the sign of $k_z$), we assume that the waves arrive only from one side of the plane.

We next assume that an infinite number of plane wave compose the sound field, covering all real values of $k_x$ and $k_y$, from $-\infty$ to $\infty$ (although as discussed in Williams[1] we expect $w(k_x, k_y)$ to be zero outside the circle $k_x^2 + k_y^2 = k^2$ if only plane wave are considered). The total pressure on the plane can now be written as a double integral over $k_x$ and $k_y$, as follows (see Williams[1] page 32):

$$p(x, y) = \frac{1}{4\pi^2}\int_{-\infty}^{\infty}\int_{-\infty}^{\infty} w(k_x, k_y)e^{j(k_x x + k_y y)}dk_x dk_y \tag{39}$$

Note that $w$ in Eq. (39) now denotes sound pressure amplitude density (with respect to $k_x$ and $k_y$), although as discussed above for the spherical configuration, the distinction between $w$ in Eqs. (39) and (38) is not made for notation simplicity. The derivation presented by Williams[1](page 32) does not make this distinction as well.

Equation (39) has the form of an inverse Fourier transform. The corresponding forward transform can therefore be readily calculated as[1]:

$$w(k_x, k_y) = \int_{-\infty}^{\infty}\int_{-\infty}^{\infty} p(x,y)e^{-j(k_x x + k_y y)}dxdy \tag{40}$$

This result shows that using the Fourier integral, the total pressure over the infinite plane $z = 0$ can be used to calculate the amplitude (density) and directivity of all plane waves contributing to that pressure, i.e. plane wave decomposition. The result for a rigid plane will be similar as the presssure on the plane will be doubled compared to an open plane. Considering a plane wave as in Eq. (38) but with a unit amplitude propagating in the direction $(k_{k0}, k_{y0})$, and substituting in Eq. (40), the directivity for a single plane wave is given by:

$$w(k_x, k_y) = \int_{-\infty}^{\infty}\int_{-\infty}^{\infty} e^{j(k_x x + k_y y)}e^{-j(k_{x0} x + k_{y0} y)}dxdy = 2\pi\delta(k_x - k_{x0}, k_y - k_{y0}) \tag{41}$$

This is derived from the fact the the Fourier transform of an exponential is a delta function[18]. This shows that plane wave decomposition can be achieved perfectly with an infinite plane, and that the pressure on the plane and the directivity of the plane waves form a Fourier pair. This is in contrast to the spherical configuration where the relation was found to be that of convolution.

Since the measurement plane is never infinite in practice, it is important to derive the effect of the finite aperture. This effect can be described mathematically as a multiplication of the pressure over the entire plane with a spatial rectangle window function, $\Pi$, where

$$\Pi(x,y) = \begin{cases} 1 & -1/2 \leq x, y \leq 1/2 \\ 0 & otherwise \end{cases} \tag{42}$$

The directivity of a finite aperture array of dimensions $L_x$ and $L_y$ can be calculated similar to Eq. (41), for a signle plane wave propagating to $(k_{x0}, k_{y0})$, as:

$$\begin{aligned} w_L(k_x, k_y) &= \int_{-\infty}^{\infty}\int_{-\infty}^{\infty} \Pi(x/L_x, y/L_y)e^{j(k_x x + k_y y)}e^{-j(k_{x0} x + k_{y0} y)}dxdy \\ &= L_x L_y \delta(k_x - k_{x0})\delta(k_y - k_{y0}) * \mathtt{sinc}(k_x L_x/2)\mathtt{sinc}(k_y L_y/2) \\ &= L_x L_y \mathtt{sinc}((k_x - k_{x0})L_x/2)\mathtt{sinc}((k_y - k_{y0})L_y/2) \end{aligned} \tag{43}$$

where $*$ denotes (2D) convolution, and the effect of the finite aperture is represented as convolution of a sinc function with the "ideal" directivity of a delta function. With a directivity of a sinc function, plane wave decomposition cannot be achieved perfectly. The resolution or the width of the main lobe of the sinc function depends on frequency, the aperture, and the actual direction of arrival $(k_{x0}, k_{y0})$. The dependence on the direction of arrival can be illustrated using the Ewald sphere construction, where the sinc function on the $(k_x, k_y)$ plane is mapped to a directivity function in spherical coordinates (see Williams[1] page 43).

To simplify the analysis of resolution, we assume that $L_x = L_y = L$ and that $k_{x0} = k_{y0} = 0$, i.e. direction perpendicular to the plane. The first zeros of the sinc function in this case form a square confined by $k_x = k_y = \pm 2\pi/L$, while its peak points to $\theta = 0$ $(k_x = k_y = 0)$. We further simplify the analysis by approximating the square formed by the first zeros of the sinc function by an inner circle of radius $\sqrt{k_x^2 + k_y^2} = 2\pi/L$. Writing $k_x = k \sin\theta \cos\phi$ and $k_y = k \sin\theta \sin\phi$, we get an approximation for the position of the zeros:

$$\sin\theta_0 \approx \frac{2\pi}{kL} \tag{44}$$

For planes apertures which are much larger then a wavelength, $kL \gg 2\pi$, we can further approximate $\sin\theta_0$ by $\theta_0$, and the width of the main lobe, or resolution, is approximated by:

$$2\theta_0 \approx \frac{4\pi}{kL} \tag{45}$$

The dependence on $\phi$ is less clearly defined. There will be little dependence on $\phi$ for small $\theta$, while for larger $\theta$ the value of the sinc function will be small anyway.

The width of the main lobe, or resolution, approximated by Eq. (45) for the plane configuration, can be compared to Eq. (36) for the spherical configuration. These are similar when $L$, the width of the plane, is comparable to $2a$, the diameter of the sphere. This shows that when imposing finite size constraints on the plane, and finite order constraint (which relate to the sphere size) on the sphere, both provide similar spatial resolution for plane wave decomposition.

Table II illustrates the spatial resolution in plane wave decomposition by showing $2\Theta_0$ for the sphere and $2\theta_0$ for the plane as a function of sphere diameter and plane aperture. The table shows that high harmonic order, or spheres and planes of large dimensions are

required to achieve high resolution in plane wave decomposition.

## VII. EXAMPLE: PLANE WAVE DECOMPOSITION

An example of plane wave decomposition given the sound pressure on a sphere is presented in this section to illustrate the theoretical results of this paper. A single frequency sound field around a rigid sphere of radius $r = a$, with $ka = 5$, is considered. The sound field is composed of five plane waves. Fig. 8 illustrates the direction of arrival of each wave and Table III shows their amplitude.

The spherical Fourier coefficients of the pressure on the sphere due to each of the waves was calculated using Eq. (22), and the spherical Fourier coefficients of the total sound pressure on the sphere calculated as the sum of the five sets of coefficients. As $ka = 5$, the Fourier coefficient were truncated at $N = 10$ ($n \leq 10$). Figure 2a shows that the higher order harmonics (the magnitude of $\tilde{b}_n$ for $n > 10$) is smaller by at least 40 dB in this case. Given $N = 10$ and $\tilde{p}_{nm}$ the spherical Fourier transform of the total sound on the sphere, the directivity $w_N$, or plane wave decomposition was calculated using Eq. (32).

Figure 9 illustrates the total pressure on the sphere due to the five plane waves. As can be seen it is not clear where the wave are arriving from given the total pressure. Figure 10 shows similar plots for $w_N$, the plane waves amplitudes after plane wave decomposition was performed, where the directions of arrival are illustrated more clearly. Table II shows that for $N = 10$ the spatial resolution, or width of the main lobe, is 36°. The waves denoted by (iv) and (v) in Table III are well separated in Fig. 10, as their spatial separation is 40°. However, the two waves denoted by (ii) and (iii), separated by only 15°, cannot be resolved in Fig. 10, as their separation is smaller then the resolution. Figure 11 shows a plot similar to that of Fig. 10b, only here a higher order of $N = 50$ was used for plane wave decomposition, corresponding to a spatial resolution of 7.2° (see Table II). All five waves can now be resolved with this improved resolution.

This example illustrated how plane wave decomposition can be achieved using spherical convolution and how finite harmonic order limits the spatial resolution of plane wave decomposition.

## VIII. CONCLUSIONS

This paper presented the theory and an example of plane wave decomposition given the pressure on a sphere, and the limitations of spatial resolution when a band-limited analysis in the spherical Fourier transform domain is employed. The results were compared to that of planar configuration. It was shown that while the amplitude of the plane waves composing the sound field and the pressure on the plane form a Fourier transform pair, for spherical configuration the waves amplitude and the pressure on a sphere are related through spherical convolution. It was further shown that under practical constraints, both the planar and spherical configurations have similar spatial resolution.

The results developed in this paper can be useful in the analysis and design of spherical microphone arrays for sound field analysis or other sound field measurements. Spherical microphone arrays that aim to perform plane wave decomposition can compute an approximation of the spatial distribution of the plane waves amplitudes by directly performing convolution as described in this paper, or by computing convolution through the spherical Fourier transform. This is in contrast to current methods which use beamforming for directive sound field analysis or measurement. Spherical convolution based microphone arrays and their use for sound field analysis are the subject of current research.

## ACKNOWLEDGEMENTS

Valuable discussions which initiated the research presented in this paper took place at the Research Lab of Electronics, MIT, with Julie E. Greenberg and other members of the Sensory Communication Group, while the author was on a Sabbatical leave at MIT, which was supported by EPSRC grant GR/R90048/01 and the Royal Academy of Engineering grant reference IJB/AH/ITG 01-658.

---

[1] E.G. Williams, *Fourier acoustics: sound radiation and nearfield acoustical holography* (New York, Academic Press, 1999).

[2] H.F. Silverman, W.R. Patterson III, and J.L. Flanagan, "The huge microphone array ," IEEE Trans. Concurrency, 6, 36-46 (1998).

[3] H.F. Silverman, W.R. Patterson III, and J. Sachar, "Factor affecting the performance of large-aperture microphone arrays," J. Acoust. Soc. Am. 111(5.1), 2140-2157 (2002).

[4] E. Hulsebos, D. De Vries, and E. Bourdillat, "Improved microphone array configurations for auralizations of sound fields by wave-field synthesis," J. Audio Eng. Soc. 50(10), 779-790 (2002).

[5] A.J. Berkhout, D. De Vries, and P. Vogel, "Acoustic control by wave field synthesis ," J. Acoust. Soc. Am. 93(5), 2764-2778 (1993).

[6] A.J. Berkhout, D. De Vries, and J.J. Snoke, "Array technology for acoustic wave field analysis in enclosures," J. Acoust. Soc. Am. 102(5.1), 2757-2770 (1997).

[7] H. Nomura, and H. Miyata, "Microphone arrays for improving speech intelligibility in a reverberant or noisy space," J. Audio Eng. Soc. 41(10), 771-781 (1993).

[8] J. Meyers, "Beamforming for a circular microphone array mounted on spherical shaped objects," J. Acoust. Soc. Am. A 15(3), 636-651 (2001).

[9] J. Meyers and G.W. Elko, "A highly scalable spherical microphone array based on an orthonormal decomposition of the soundfield," Proceedings of ICASSP 2002, vol. II, 1781-1784 (2002).

[10] T.D. Abhayapala and D.B. Ward, "Theory and design of high order sound field microphones using spherical microphone array," Proceedings of ICASSP 2002, vol. II, 1949-1952 (2002).

[11] J. Meyers and G.W. Elko, "A spherical microphone array for spatial sound recordings," J. Acoust. Soc. Am. 111(5.2), 2346 (A) (2002).

[12] B.N. Gover, J. G. Ryan and M. R. Stinson, "Microphone array measurement system for analysis of directional and spatial variations of sound fields," J. Acoust. Soc. Am. 112(5), 1980-1991 (2002).

[13] J. R. Driscoll, and D. M. Healy Jr., "Computing Fourier transforms and convolutions on the 2-sphere." Advances in Applied Mathematics, 15, 202-250 (1994).

[14] G. Arfken and H. J. Weber, *Mathematical methods for physicists* 5th ed. (San Diego, Academic Press, 2001).

[15] Wolfram Research on-line publication of mathematical functions, http://www.function.wolfram.com (2003).

[16] B.D. Wandelt andK.M. Gorski, "Fast convolution on the sphere," Physical Review D, 63, 123002, 1-6 (2001).

[17] I. S. Gradshteyn and I. M. Ryzhik, *Tables of integrals, series, and products* (New York, Academic Press, 1980).

[18] A. V. Oppeneim, A. S. Willsky, with S. H. Nawab, *Signals and Systems* (New Jersey, Prentice Hall, 1997).

| Order $N$ | Directivity $w_N(z)$, $z = \cos\Theta$ |
|---|---|
| 0 | $\frac{1}{4\pi}$ |
| 1 | $\frac{1}{4\pi}(3z + 1)$ |
| 2 | $\frac{1}{4\pi}\frac{3}{2}(5z^2 + 2z - 1)$ |
| 3 | $\frac{1}{4\pi}\frac{1}{2}(35z^3 + 15z^2 - 15z - 3)$ |
| 4 | $\frac{1}{4\pi}\frac{5}{8}(63z^4 + 28z^3 - 42z^2 - 12z + 3)$ |
| 5 | $\frac{1}{4\pi}\frac{6}{16}(231z^5 + 105z^4 - 210z^3 - 70z^2 + 35z + 5)$ |

TABLE I: Directivity function $w_N$ for several orders $N$.

| Sphere $2\Theta_0$ | $N$ | $2a(\lambda)$ |
|---|---|---|
| Plane $2\theta_0$ | | $L$ $(\lambda)$ |
| 360.0° | 1 | 0.3 |
| 180.0° | 2 | 0.6 |
| 72.0° | 5 | 1.6 |
| 36.0° | 10 | 3.2 |
| 12.0° | 30 | 9.5 |
| 7.2° | 50 | 15.9 |
| 3.6° | 100 | 31.8 |
| 1.2° | 300 | 95.5 |

TABLE II: Resolution, or width of main lobe for the spherical configuration ($2\Theta_0$) and planar configuration ($2\theta_0$) as a function of harmonic order $N$, diameter of measurement sphere ($2a$) or plane aperture ($L$).

| | $\theta_l$ | $\phi_l$ | $\lvert w(\theta_l, \phi_l)\rvert$ | $\angle w(\theta_l, \phi_l)$ |
|---|---|---|---|---|
| (i) | 20° | 200° | 1 | 0° |
| (ii) | 45° | 270° | 1 | 20° |
| (iii) | 60° | 270° | 1 | 80° |
| (iv) | 120° | 210° | 1 | 180° |
| (v) | 120° | 250° | 1 | 270° |

TABLE III: Direction of arrival $(\theta_l, \phi_l)$, magnitude and phase of each of the five plane waves.

## Figure captions

Fig. 1: Cartesian and spherical coordinate systems.

Fig. 2: Magnitude of $\tilde{b}_n(kr, ka)$ for (a) rigid sphere with $kr = ka$, (b) open sphere, with orders of n=0 to 4 denoted on the figures.

Fig. 3: Magnitude of $\tilde{b}_n(kr, ka)$ for a rigid sphere as a function of $n$, for $ka = 1$, 5 and 10 as denoted on the figure, and $kr = ka$.

Fig. 4: Magnitude of $b(\theta, \phi)$ for a rigid sphere, $kr = ka = 5$, $n \leq 10$, (a) three-dimensional plot on the unit sphere, and (b) two-dimensional plot as a function of $(\theta, \phi)$.

Fig. 5: Magnitude of $\beta(\theta, \phi)$ for a rigid sphere, $kr = ka = 5$, $n \leq 10$, (a) three-dimensional plot on the unit sphere, and (b) two-dimensional plot as a function of $(\theta, \phi)$.

Fig. 6: Normalized directivity $w_N(\Theta)$ for a plane wave as a function of order $N$.

Fig. 7: The first zero $w_N(\Theta_0) = 0$ as a function of $N$, and the approximation $\Theta_0 \approx \pi/N$.

Fig. 8: Direction of arrival of the plane waves as described in Table III, illustrated on a two-dimensional plot as a function of $(\theta, \phi)$.

Fig. 9: Magnitude of the sound pressure level $p_N(\theta, \phi)$ on the sphere due to the plane waves described in Table III, (a) three-dimensional plot on the unit sphere, and (b) two-dimensional plot as a function of $(\theta, \phi)$.

Fig. 10: Directivity $w_N$ of the sound field due to the plane waves described in Table III and Fig. 8, calculated for $n \leq 10$, illustrated using (a) three-dimensional plot on the unit sphere, and (b) two-dimensional plot as a function of $(\theta, \phi)$.

Fig. 11: Directivity $w_N$ of the sound field due to the plane waves described in Table III and Fig. 8, calculated for $n \leq 50$, illustrated using two-dimensional plot as a function of $(\theta, \phi)$.

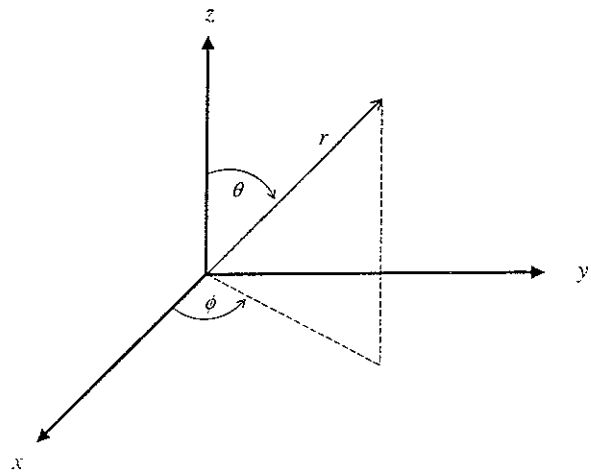


FIG. 1: Cartesian and spherical coordinate systems.

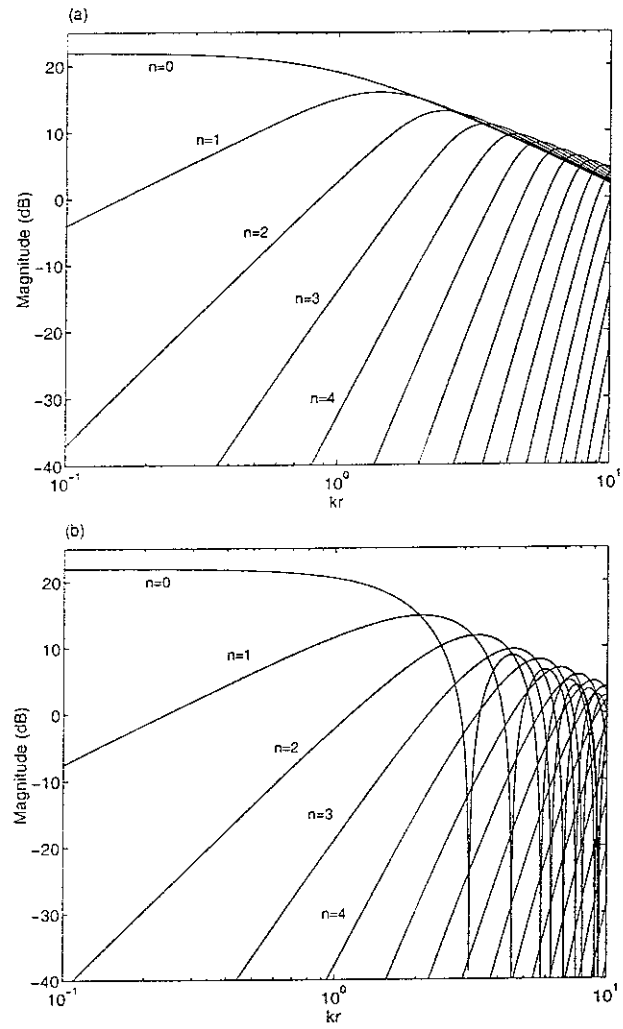


FIG. 2: Magnitude of $\tilde{b}_n(kr, ka)$ for (a) rigid sphere with $kr = ka$, (b) open sphere, with orders of n=0 to 4 denoted on the figures.

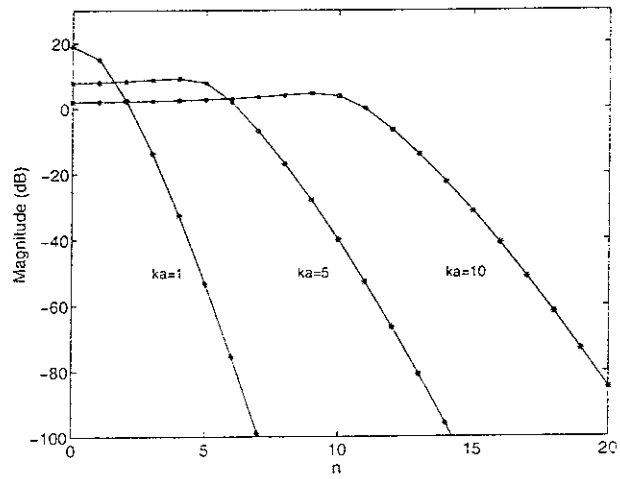


FIG. 3: Magnitude of $\tilde{b}_n(kr, ka)$ for a rigid sphere as a function of $n$, for $ka = 1$, 5 and 10 as denoted on the figure, and $kr = ka$.

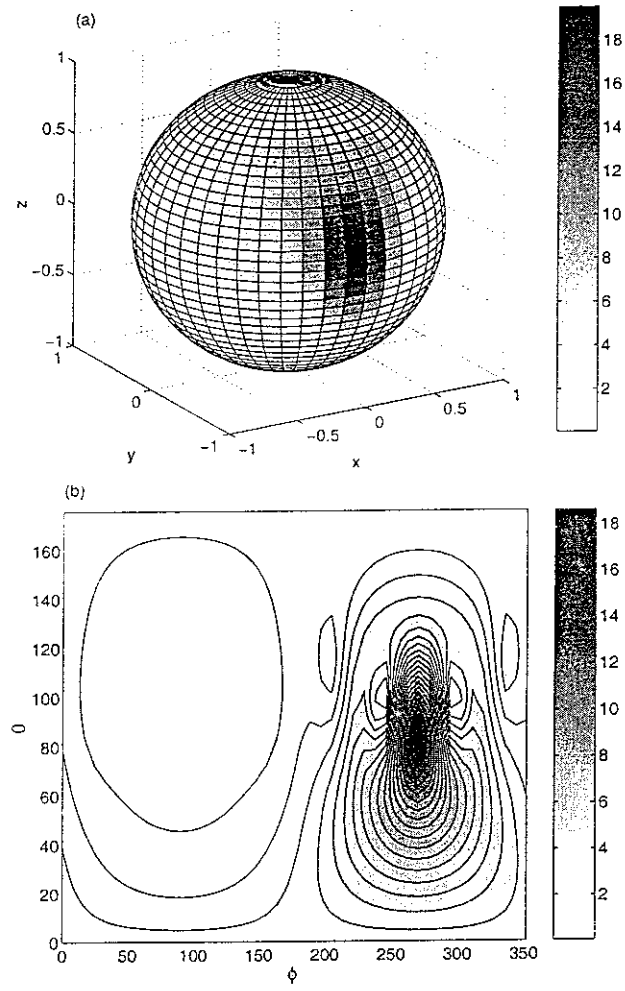


FIG. 4: Magnitude of $b(\theta, \phi)$ for a rigid sphere, $kr = ka = 5$, $n \leq 10$, (a) three-dimensional plot on the unit sphere, and (b) two-dimensional plot as a function of $(\theta, \phi)$.

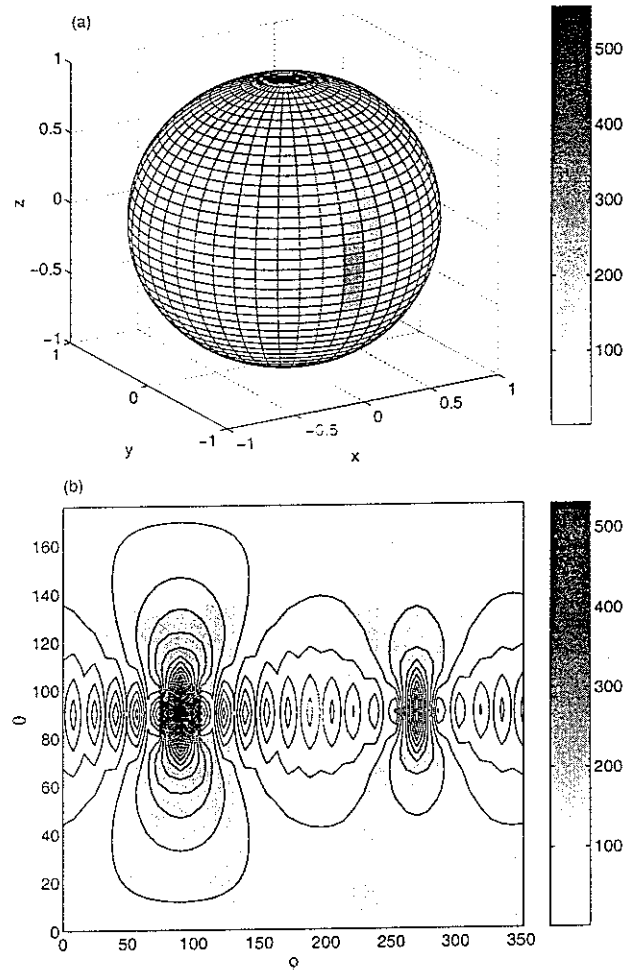


FIG. 5: Magnitude of $\beta(\theta, \phi)$ for a rigid sphere, $kr = ka = 5$, $n \leq 10$, (a) three-dimensional plot on the unit sphere, and (b) two-dimensional plot as a function of $(\theta, \phi)$.

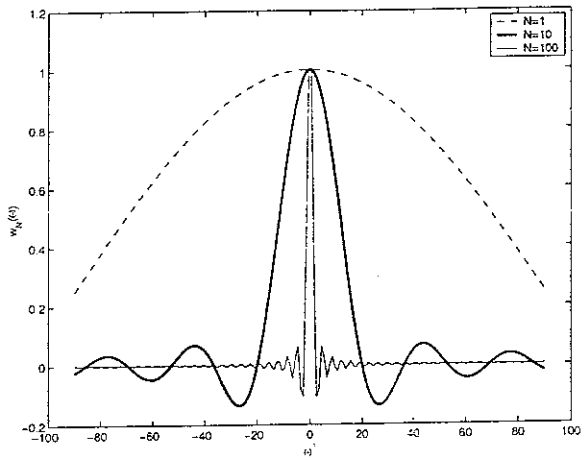


FIG. 6: Normalized directivity $w_N(\Theta)$ for a plane wave as a function of order $N$.

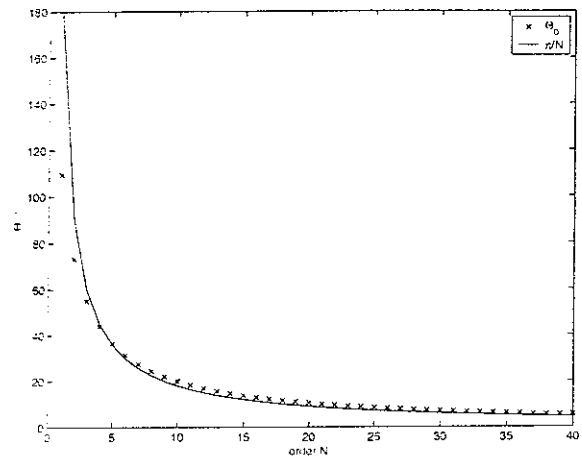


FIG. 7: The first zero $w_N(\Theta_0) = 0$ as a function of $N$, and the approximation $\Theta_0 \approx \pi/N$.

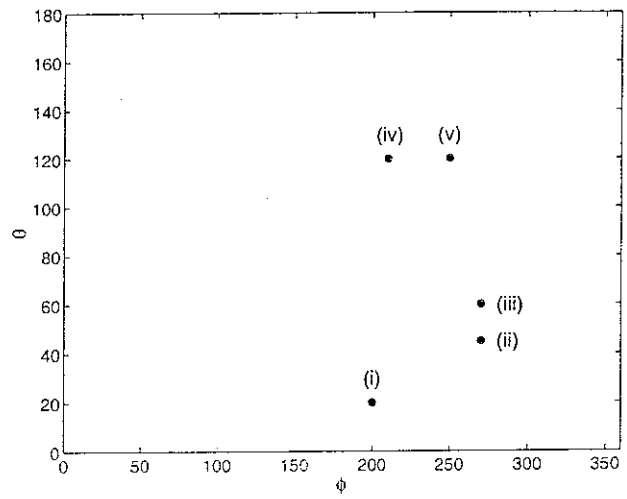


FIG. 8: Direction of arrival of the plane waves as described in Table III, illustrated on a two-dimensional plot as a function of $(\theta, \phi)$.

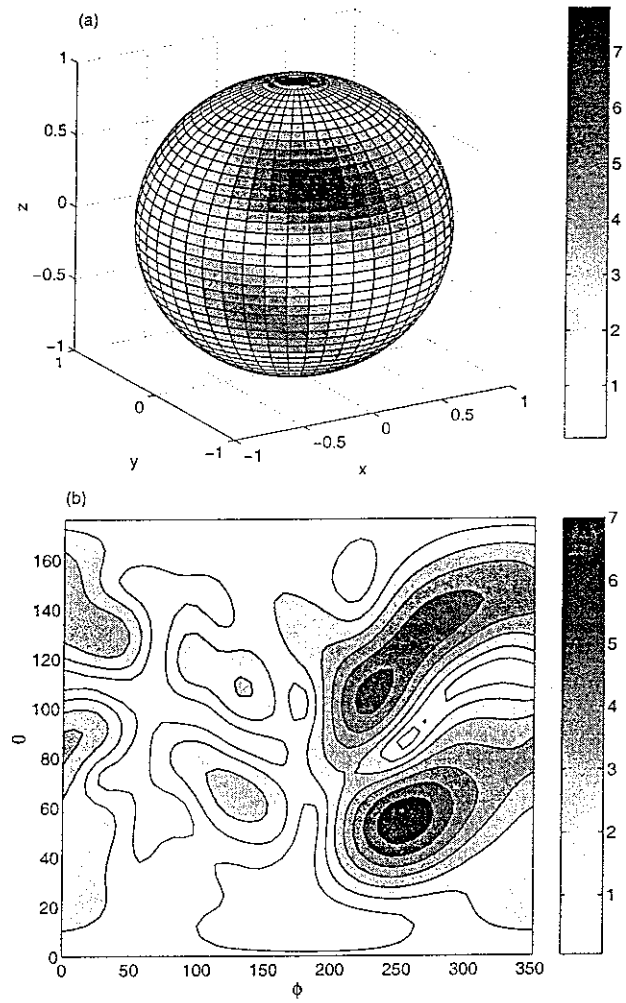


FIG. 9: Magnitude of the sound pressure level $p_N(\theta, \phi)$ on the sphere due to the plane waves described in Table III, (a) three-dimensional plot on the unit sphere, and (b) two-dimensional plot as a function of $(\theta, \phi)$.

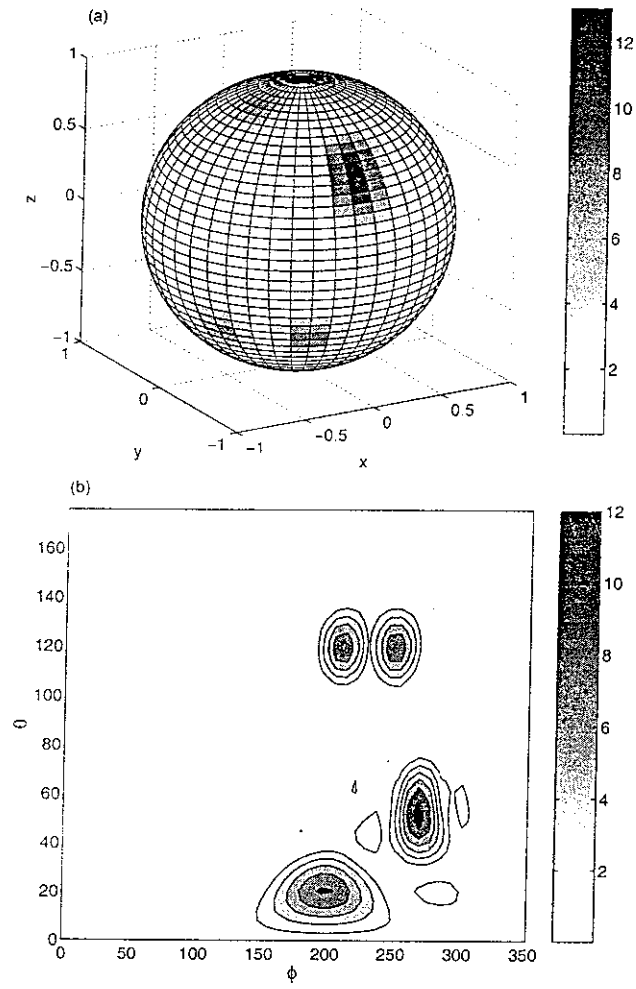


FIG. 10: Directivity $w_N$ of the sound field due to the plane waves described in Table III and Fig. 8, calculated for $n \leq 10$, illustrated using (a) three-dimensional plot on the unit sphere, and (b) two-dimensional plot as a function of $(\theta, \phi)$.

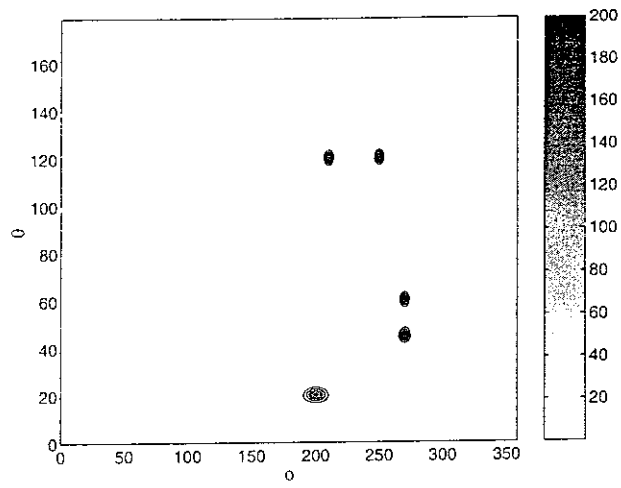


FIG. 11: Directivity $w_N$ of the sound field due to the plane waves described in Table III and Fig. 8, calculated for $n \leq 50$, illustrated using two-dimensional plot as a function of $(\theta, \phi)$.